Sustainable Energy & Fuels

ROYAL SOCIETY OF CHEMISTRY

PAPER

View Article Online
View Journal | View Issue

Cite this: *Sustainable Energy Fuels*, 2026, **10**, 375

Optimising supercritical water gasification of biomass: exploring heating strategy through a quantitative kinetic modelling approach

Robert Sait-Stewart, Leo Lue and Jun Li *

Supercritical water gasification (SCWG) offers a promising method to process wet biomass and realise its full potential as a renewable energy source, as well as to efficiently treat waste biomass streams. To optimise this technology for more energy-efficient operations, this work provides a comprehensive investigation into the impact of heating rate and profile on the SCWG of biomass. Using an upgraded SCWG kinetic model, process simulations were used to explore the potential in enhancing syngas yields and carbon gasification efficiency, and mitigating char formation by changing sub-critical heating rates and heating profiles (*e.g.*, linear, accelerating, decelerating). Reducing sub-critical heating rates from hundreds to a few °C min^{-1} is found to be beneficial for increasing the yield of H_2 from the SCWG of cellulose and hemicellulose in particular, where the increase in H_2 yield exceeded 10 °C min^{-1}. The dry mass fraction of char produced from lignin SCWG could be reduced from roughly 30 °C min^{-1} to 20 °C min^{-1} by increasing the sub-critical heating rate by two orders of magnitude to 690 °C min^{-1}. The effect of sub-critical heating profile was less significant, with the only notable trend being increased lignin-derived char with a decelerating sub-critical heating profile. This work shows the potential improvements that could be made to SCWG by tailoring the sub-critical heating regime in accordance with the feedstock to optimise syngas yields and char formation.

Received 27th May 2025
Accepted 18th November 2025

DOI: 10.1039/d5se00755k

rsc.li/sustainable-energy

1 Introduction

Biomass wastes arise in various forms, including wastewater and sewage sludge (WSS), organic fraction of municipal solid waste (OFMSW), agricultural waste (AW), and food industry waste (FIW).[1] A significant portion of these biomass wastes are wet in their original forms, being composed of as much as 80 wt% water in some cases.[2] Wet biomass wastes present a unique set of challenges in their processing, and are viewed as materials which pose problems in their management and disposal. These waste materials are rich in organics (*e.g.*, cellulose, hemicellulose, protein, and lipids) and other useful nutrients (*e.g.*, phosphorous). Forecasting suggests the UK may have access to over 9400 GWh worth of food waste by 2030.[3] If the full value of waste biomass could be recovered, these materials could become a sustainable feedstock for producing bioenergy to help meet net-zero emission targets, but also a source of fertiliser nutrients to help support agriculture. Processing wet biomass wastes using conventional thermochemical treatment options (*e.g.*, pryolysis, gasification, *etc.*) is severely hindered by the requirement of an energy-intensive pre-drying stage.[4,5]

Hydrothermal processing refers to a group of three high-pressure, high-temperature thermochemical conversion processes which are differentiated based upon their operating conditions and product distribution. In increasing operating temperature order, hydrothermal carbonisation (HTC), liquefaction (HTL), and gasification (HTG) produce predominantly solid, liquid, and gas biofuel products, respectively.[6] Operating at temperatures in the range of 360 °C to 700 °C, HTG is capable of rapidly and efficiently (>90%) converting wet biomass into syngas.[7] When operating conditions are in-excess of the critical point of water (22.1 MPa and 374 °C), HTG boasts its highest conversion efficiency and the ability to produce a H_2-rich fuel in a process also termed supercritical water gasification (SCWG).[6,8]

Fig. 1 shows a pressure *versus* temperature phase diagram for water. The shaded region shows pressures deployed during SCWG, which are typically achieved through pumping of the process stream prior to heating.[7] A series of annotations are included on the phase diagram which demonstrate the influence temperature has on controlling the major products formed during various hydrothermal processes.

Temperature is the most influential SCWG process variable.[2,9] At temperatures below or near the critical point, the gasification process is governed by the formation of H^+ and OH^- *via* the ionic products of water mechanism which favors the formation of CH_4;[2,10] while increasing the temperature beyond 500 °C slows the ionic products mechanism and

University of Strathclyde, Department of Chemical and Process Engineering, 75 Montrose Street, Glasgow, G1 1XJ, UK. E-mail: jun.li@strath.ac.uk

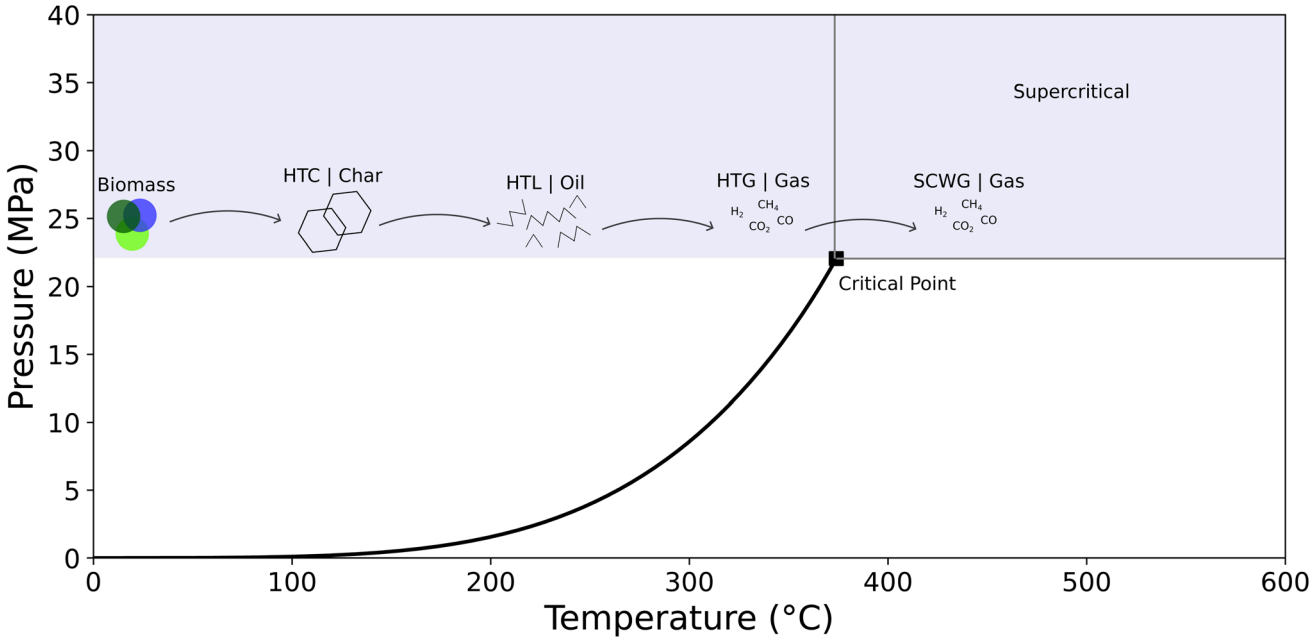

Fig. 1 Pressure *versus* temperature phase diagram for water showing the operating conditions and main products for different hydrothermal processes.

expedites the formation of hydronium ions (H_3O^+). The resulting reduction to system pH changes the gasification mechanism to becoming free-radical controlled, which favors the formation of H_2 and increases the gasification efficiency compared to the ionic mechanism.[2,10] Catalysts can be used to help lower the temperature required to achieve targeted H_2 yields or gasification efficiency.[7]

During SCWG, a pre-heater is required to heat the pressurised process stream closer to the desired reaction temperature.[7] Whilst its primary function is to act as a heat exchanger, the pre-heater also represents a low-temperature, sub-critical reaction region where the initial degradation of biomass into chars and bio-oils will commence. There is very little information available regarding how the operation of the pre-heater affects the overall production of syngas. Given that the purpose of the pre-heater is to provide a temperature change, the main user-changeable operating variable is the heating rate. Matsumura *et al.*[11] conducted an experimental investigation into heating rates and found that for both a glucose and a cabbage feedstock, faster heating rates in the range of 10–30 °C s^{-1} promoted greater gasification efficiencies. More recent experimental work completed by Farobie *et al.*[12] using a mixed glucose/guaiacol feedstock found that increasing heating rate improved gasification efficiency up until around 25 °C s^{-1}, after which subsequent increments to the heating rate decreased the gasification efficiency.

The commercialisation of SCWG is hindered by several key challenges including char formation, salt plugging/corrosion, and a high energy demand.[2,13,14] The limited but valuable experimental data available shows that heating rate can influence the transformation of biomass into syngas during SCWG. This work theorises that SCWG heating regimes could be tailored according to the composition of a specific biomass feedstock in order to enhance the formation of syngas, suppress char formation, and ultimately improve the economic viability of the process. In addition to the heating rate, non-linear heating profiles are also studied within this work to investigate if and how they can be used to optmise SCWG.

This work aims to holistically analyse the affect of operational heating rate and profile in the sub-critical region on the SCWG of biomass. The predicted yields of syngas species (CO, CO_2, CH_4 and H_2); the formation of char; and the generation of key intermediate compounds are used as key indicators of the process and are thoroughly analysed and discussed. The results provide a comprehensive guide for optimal SCWG operations to help tailor heating regimes based on the requirement of feedstock variation to maximise syngas production and process efficiency.

To conduct the systematic analysis of heating regime, an upgraded kinetic model based upon that of Yakaboylu *et al.*[15] was used. This model used 55 and 74 sub- and supercritical reactions, respectively, and characterises the wet biomass feedstock using four major constituent compounds: cellulose, hemicellulose, lignin, and protein. The modelling chapter to follow acts as a methodology where the kinetic model is first qualitatively described and then the modifications made in this work are explicitly described and justified. The results chapter is divided into two sections to separately demonstrate the influence that sub-critical heating rate and profile has on SCWG.

2 Modelling concepts and development

The full kinetic model including Arrhenius parameters, molecule names, and reaction IDs is included in the SI. Cellobiose,

xylose, guaiacol, and aspartic acid are used in the model to represent the major organic constituents of wet biomass: cellulose, hemicellulose, lignin, and protein, respectively. In each case, the model compound is a primary hydrolysis product of the biomass component.

2.1 Modifications to the model

The model reported by Yakaboylu *et al.*[15] was able to reproduce the carbon gasification efficiency of biomass, however there is a notable disparity in the underpredictions of the yields of H_2, and overprediction of CH_4. It was suggested that these inaccuracies were likely due to incorrect lignin gasification stoichiometries. Given that the biomass mixture of wood sawdust and carboxymethylcellulose (CMC) used for lignocellulosic validation is composed mainly of cellulose, it is unlikely that the disparity in H_2 and CH_4 yields can be attributed solely to inaccurate lignin gasification stoichiometry. This work also considers the possibility that the main source of error is from the cellulose decomposition mechanism.

Acetic acid is a key intermediate during the SCWG of cellulose which is formed *via* five separate pathways from molecules including erythrose and levoglucosan. Acetic acid gasifies directly *via* only one route in the global mechanism (`aa.ga`) to form CO_2 and CH_4. On the other hand, formic acid is produced from the decomposition of 5-HMF (`5.1f`) only and will gasify directly to produce CO_2, CO and H_2 (`fa.ga1`, `fa.ga2`). It is therefore theorised that the kinetic model over and underpredicts the formation of acetic and formic acids, respectively, which subsequently causes inaccurate yields of CH_4 and H_2.

The basis for this hypothesis comes from the experiments of Kabymela *et al.*[16] Despite detecting both formic and acetic acids from the hydrothermal decomposition of these two intermediates, only acetic acid was included as a product in the reference model. Excluding formic acid as a product from these reactions was possibly due to the uncertainty in reaction stoichiometry, which is not yet well understood.[17] It is well known that of both formic acid and acetic acids are major products from the hydrothermal decomposition of erythrose, levoglucosan, and other cellulitic materials.[16–18]

To further improve the kinetic model and allow for formic acid production from erythrose and levoglucosan, the reactions `e.acid` and `a.acid` were modified as shown in Table 1.

Due to ambiguity in the mechanism, the new stoichiometries of `e.acid` and `a.acid` were estimated to give roughly equal yields of formic and acetic acid. It was also necessary to balance the equation using H atoms on the product side of both reactions.

Another modification to the model related to the Arrhenius parameters for xylose decomposition reactions. Yakaboylu *et al.*[15] cites Jing and Lu[19] as the source of activation energies and pre-exponential factors for xylose decomposition in the reference model. However, a discrepancy exists in the Arrhenius parameters listed by the two authors – as shown in Table 2. The reference model kinetic data predicts xylose to be very resistant to decomposition in the sub-critical region, with only 2 mol% conversion achieved under normal operating conditions. This is in disagreement with the work of Jing and Lu,[19] who observed 95.8% conversion of xylose after 50 min at 220 °C. Other works have also demonstrated that xylose behaves similarly to glucose under hydrothermal conditions.[8] The results of this work show the model to predict that glucose decomposes readily in supercritical conditions, and thus its expected that xylose would to. The kinetic model of this work was therefore updated to use the kinetic data from Jing and Lu[19] as it produced an expected, gradual conversion of xylose into furfural, glyceraldehyde, and methyl formate in the sub-critical reactor.

2.2 Cellulose

Cellulose comprises around 40–55 $wt\%_{dry}$ of lignocellulosic material and is a major component in wet biomass.[14] Glucose, erythrose, and glycolaldehyde are the main products formed from the primary hydrolysis of cellobiose, and are generated directly though reaction 3 or *via* a glucosyl intermediate in one of the two-step reactions, `1•ge.g` or `2•gg.g`. Glucose decomposes further into either erythrose (`g.e`) or one of four other secondary products: levoglucosan (`g.a`), 5-HMF (`g.5`), fructose (`g.f`), or glyceraldehyde (`g.gly`). Pyruvaldehyde is then formed from glyceraldehyde directly (`gly.p`) or *via* dihydroxyacetone (`gly.dih•dih.p`). The intermediates formed thus far decompose into a mixture composed of predominantly acetic and lactic acid; with the former being produced from eryhthrose (`e.acid`), glycolaldehyde (`glyco.acid`), and levoglucosan (`a.acid`), and lactic acid being produced from fructose (`f.acid`) and pryuvaldehyde (`p.acid`). These simple organic compounds will either gasify directly or after undergoing further decomposition reactions. Acetic acid for example gasifies to CO_2 and CH_4 (`aa.ga`) in exclusively supercritical conditions, whilst formic acid will be gasified into a mixture of CO_2, H_2, CO and H_2O (`fa.ga1` and `fa.ga2`) in both the sub- and supercritical region. Lactic acid decomposes *via* a pathway composed of 8 reactions and 3 intermediates (acyrlic acid, 3-HPA, and acetaldehyde) to produce 3 simple organic acids: acetic, propionic, and glycolic. In supercritical conditions, propionic and glycolic acid gasify to form mixtures of CO and H_2, and CO_2 and H_2, respectively formalehyde also gasifies in the supercritical region to produce

Table 1 Updated kinetic model reactions

Reaction	Reference model	This work
`e.acid`	$C_4H_8O_4 \rightarrow 2C_2H_4O_2$	$C_4H_8O_4 + 2H_2O \rightarrow C_2H_4O_2 + 2CH_2O_2 + (4H)$
`a.acid`	$C_6H_{10}O_5 + H_2O \rightarrow 3C_2H_4O_2$	$C_6H_{10}O_5 + 3H_2O \rightarrow 2C_2H_4O_2 + 2CH_2O_2 + (4H)$

Table 2 Arrhenius parameters for hemicellulose decomposition in sub-critical water

	Jing and Lu[19]		Yakaboylu *et al.*[15]	
	Activation energy, E_a (kJ mol^{-1})	Pre-exponential factor, A (s^{-1})	Activation energy, E_a (kJ mol^{-1})	Pre-exponential factor, A (s^{-1})
xy.fu	111.47	2.26×10^{10}	76.6	1230
xy.gm	143.14	5.03×10^{13}	153.8	7.38×10^{8}
fu.aa	58.84	1.19×10^{5}	24.2	2.95×10^{-14}

CO and H_2 (fal.ga) whereas levulinc acid decomposes into a mixture of lactic acid and acetaldehyde (levu.lacet). Furfural is the only remaining simple organic in the cellulose decomposition mechanism. In sub-critical conditions, furfural decomposes *via* fu.aa into a mixture of acetic and acrylic acid, termed water-soluble humic species (WSHS). The stoichiometry of this reaction was not specified in the reference source hence the need to group this two species under the single moniker, WSHS. Under supercritical condtions, WSHS can gasify into CO and H_2 (aa.gas), and char formation from fufural is also possible (fu.ch). The water-gas shift (WGS) reaction, which produces H_2 and CO_2 from CO and H_2O was the only "gas-phase" reaction included the model. The decomposition mechanism for cellulose is the most detailed of the four model compounds in wet biomass as it includes the most intermediates and reactions.

2.3 Hemicellulose

Hemicellulose is another major component of lignocellulosic material, comprising roughly 15–35 wt%$_{dry}$.[14] Xylose is a monomer unit and primary hydrolysis product of hemicellulose; it has a comparatively simpler decomposition pathway in the kinetic model compared to cellulose. In sub-critcal conditions, hemicellulose will decompose into furufral (xy.fu) and a mixture of glyceraldehyde and methyl formate. Like in the cellulose mechanism, furfural will produce WSHS (fu.aa) whereas glyceraldehyde will ultimately form lactic acid (p.acid) after decomposing into pyrvuladehyde (gly.p and gly.dih•dih.p). Under supercritical conditions, methyl formate decomposed into acetic acid (mf.aa); WSHS gasifies into CO and H_2 (aa.gas); and char formation can occur from furfural (fu.ch). Hemicellulose gasifies the most readily of the four biomass components, and it is expected to have high yields of H_2 and to achieve near-complete gasification.[15]

2.4 Lignin

Lignin is the remaining component in lignocellulosic biomass, typically accounting for 20–40 wt%$_{dry}$.[14] Lignin is the most complex of the three lignocellulosic materials and produces a wider distribution of products upon first decomposition. Guaiacol was selected as the lignin-representative model compound, which has also been done in other publications with the reasoning being that it has a similar structure and functional groups to lignin.

In sub-critical conditions, guaiacol forms diphenyl directly (gu.t) or *via* catechol and oCresol. Diphenyl can react to form phenol (t.p), benzene (t.b), char (t.ch) or gas (t.ga). Guaiacol can also gasify directly in sub-critical conditions (gu.ga) or form benzene(gu.b) which will go onto produce char (b.ch). In supercritical conditions, benzene can also gasify (b.ga), produce phenol (b.p), or form naphtalene (b.na) which will subsequently form char (na.ch). Phenol can also form catechol (p.c), gasify (p.ga), or form char (p.ch) in supercritical conditions.

Due to a lack of data available, the stoichiometry of the gas forming reactions in the lignin decomposition pathway were determined using a Gibbs free energy minimisation (GM) calculation (*i.e.* thermodynamically) by defining a pre-defined list of gas products: CO, CO_2, CH_4, H_2, N_2, NH_3.

2.5 Protein

Protein is an important compound to include in the SCWG model as it forms a significant component of many wet biomass wastes, such as sewage sludge and food waste.[20,21] Additionally, the production and subsequent SCWG of protein-rich microalgae is a promising area of interest in the field of 4th generation bio-refineries.[22] Protein is modelled on albumin because extensive research has been carried out using it as a model protein.[15] Aspartic acid was chosen as the model compound for protein because its decomposition products, alanine and glycine, are common amino acids obtained from the hydrolysis of albumin.

In the sub-critical region, protein will decompose into alanine (as.a) and glycine (as.g) and produce acetic acid, propionic acid and char as by-products. These amino acids decompose into ethylamine (al.et) and methylamine (g.met), respectively, with lactic acid, glycolic acid, NH_3, and CO_2 produced as side-products. In supercritical conditions, the amino acids can gasify directly ((al gas)) and (g.gas), or they will form amines which gasify (et.gas) and (met.gas). Similarly to lignin, in each reaction where direct gasification occurs the stoichiometry is calculated using a GM calculation.

2.6 Simulation approach

This work emulated a SCWG process using three plug-flow reactors in series. Labelled on Fig. 2 as SUB-HEX, SUP-HEX, and SUP-RCT, these reactors simulate (i) sub-critical reactions while linearly heating the process stream from 25 °C to 374 °C

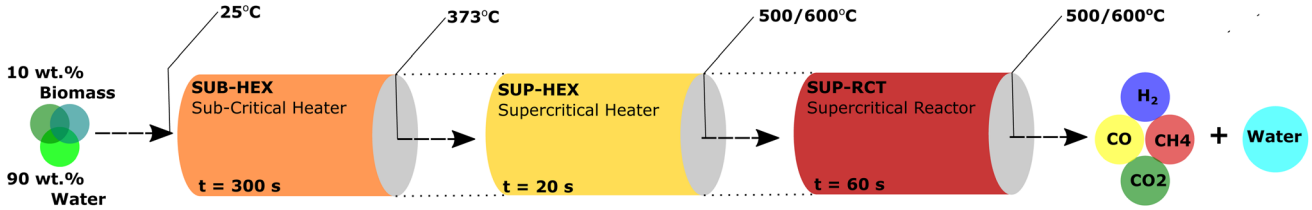

Fig. 2 The configuration of reactors used in simulations.

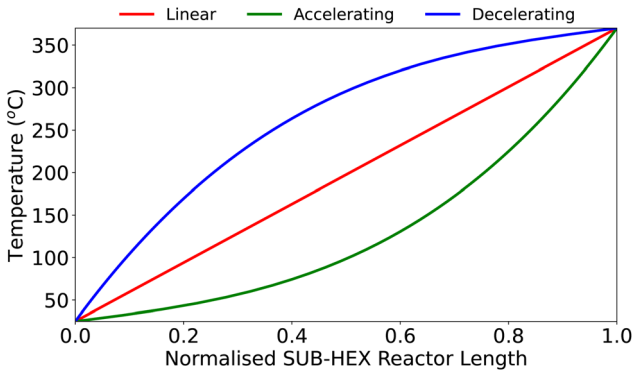

Fig. 3 Three different SUB-HEX heating profiles studied.

in 300 s, (ii) supercritical reactions while linearly heating from 374 °C to the target temperature (500 °C or 600 °C) in 20 s, and (iii) supercritical reactions while holding at the target temperature for 60 s, respectively. Along with the kinetic parameters, details describing how to reproduce the kinetic model of this work are contained in the SI.

The report focuses exclusively on the effect of sub-critical heating, and thus changes were made to the SUB-HEX reactor only. The benchmark SUB-HEX residence time of 300 s corresponds to a heating rate of 69 °C min^{-1}; this was decreased and increased by an order of magnitude to 6.9 and 690 °C min^{-1} to reveal how slower and faster heating rates in SUB-HEX affect the overall transformation of biomass into syngas. Additionally, non-linear sub-critical heating profiles were also investigated. The accelerating and decelerating profiles shown on Fig. 3 were also tested having been reproduced from Yakabolyu *et al.*[15] Temperature is widely considered the most important SCWG variable, and thus two final reaction temperatures of 500 °C and 600 °C are preseneted for each result to demonstrate how the effect of sub-critical heating rate is altered by reaction temperature.

The kinetic model was solved in Python using an ODE solver, where similarly to Yakaboylu *et al.*[15] three plug-flow reactors in series were used to emulate the reactions of a real-world, continuous SCWG plant. A standard feedstock of 1000 kg h^{-1}, 10 wt% biomass was used. Whilst the kinetic model is unaffected by changes to feedstock concentration as water is a zero-order reagent, simuations using greater concentrations of biomass would not be valid as the kinetic data was obtained from experiments using 90 wt% water or higher. Similarly, the kinetic model operates independently of pressure, but is assumed to be accurate in the range of 25 to 30 MPa.[15]

The carbon gasifiction efficiency (CGE) is a useful indicator for the evaluating the efficacy of a gasification process. It denoted the conversion efficiency of biomass carbon into gas species carbon (*i.e.*, CO, CO_2, and CH_4), and is calculated as shown in eqn (1).

$$\mathrm{CGE}(\%) = 100\left(\frac{n_{\mathrm{CO}} + n_{\mathrm{CO_2}} + n_{\mathrm{CH_4}}}{n_{\mathrm{feed}}}\right) \quad (1)$$

where n_i is the moles of carbon in species i.

3 Results and discussion

3.1 Advances and validation of the updated kinetic model

3.1.1 Lignocellulosic biomass. Validation of the kinetic model for lignocellulosic biomass (*i.e.*, cellulose, hemicellulose, and lignin only) was completed using the experimental data of Lu *et al.*[23] The residence times and heating conditions were not explicitly stated by Lu *et al.*,[23] but they were estimated based upon the high CGEs achieved. Using the same configuration of reactors presented in Fig. 2, a 4 $wt\%_{dry}$ sawdust feedstock was linearly heated across 5 s from 25 °C to 370 °C in SUB-HEX; linearly heated further to 650 °C in 3 s in SUP-HEX; and held at 650 °C for a further 39 s. The sawdust was modelled using 74.75 $wt\%_{dry}$ cellulose, 11.75 $wt\%_{dry}$ hemicellulose, and 13.25 $wt\%_{dry}$ lignin.[15]

Fig. 4 presents the results for the validation of lignocellulosic biomass. The yields of H_2, CO_2, CH_4, and CO are plotted on Fig. 4a and the CGE on Fig. 4b. The graphs show the experimental results of Lu *et al.*,[23] the Yakaboylu *et al.* model,[15] and the model of this work. The error between experimental and modelling results for the final gas phase composition was calculated. For CO_2 and CH_4, the model of this paper reduced the error from 12% to 0.5% and 43% to 22%, respectively, *versus* the Yakaboylu *et al.* model. The error in H_2 yield was maintained at roughly 29%, and the CGE error reduced marginally from 17% to 16%. Overall, it can be concluded that the kinetic model has been successfully validated for lignocellulosic biomass, and the updates improve the accuracy of gas yield predictions.

3.1.2 Protein-containing biomass. A separate experimental study was used to validate the model for protein-containing biomass. Nakamura *et al.*[24] conducted a liquefaction-gasification type treatment of a 1.97 $wt\%_{dry}$ chicken manure feedstock. The composition of the dry biomass was based upon data provided by the Phyllis[25] database; and was modelled as 12.00 $wt\%_{dry}$ cellulose, 8.76 $wt\%_{dry}$ hemicellulose, 12.14 $wt\%_{dry}$ lignin, and 43.10 $wt\%_{dry}$ protein.[15] Fig. 5 shows the

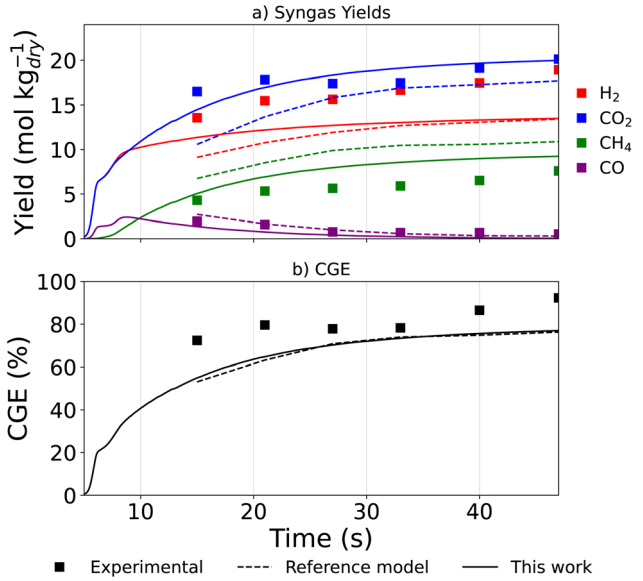

Fig. 4 Validation results for (a) gas yields and (b) CGE, from the SCWG of lignocellulosic biomass including experimental data,[23] the reference model,[15] and the results of this work.

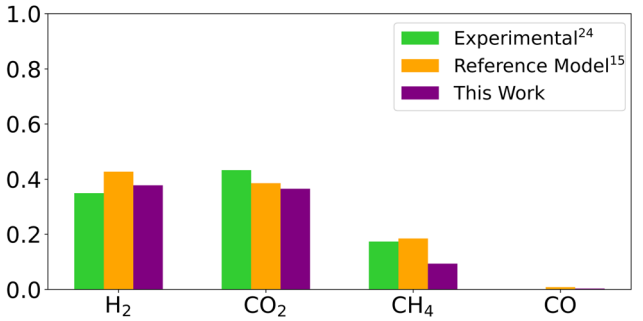

Fig. 5 Validation results for protein-containing biomass.

experimental syngas yields from Nakamura *et al.*;[24] and those predicted by the models of Yakaboylu *et al.*[15] and this work.

Fig. 5, which plots mole fractions (dry) of the product gas shows that generally the model predicts the SCWG of protein-containing biomass well. There are deviations between the experimental results and the gas yields predicted by both models. The model of this work was able to improve the estimation accuracy for H_2 yields, but worsened it CO_2 and CH_4. This error can likely be attributed to the GM calculation which was used to obtain the gasification stoichiometry for protein. Overall, there is good agreement between the experimental data and results of this model.

3.2 The effect of heating rate

3.2.1 Syngas yields and CGE. Fig. 6 shows how sub-critical heating rate influences the yields of syngas (left-hand axis) and the CGE (right-hand axis) during the SCWG of cellulose, hemicellulose, lignin, and protein. Two different cases for final reaction temperature are presented to illustrate how the product composition is affected differently by sub-critical heating rate depending on whether low temperature (500 °C) or high temperature (600 °C) gasification is being conducted. To demonstrate the affect of sub-critical heating rate on CO yield, as opposed to plotting the final product composition, Fig. 6 plots the maximum observed yields of each syngas species and the CGE. For all species bar CO, the maximum yield is equivalent to the final product composition as the kinetic model does not include reactions which consume them. However, CO is consumed *via* the only gas-phase reaction included in the model, the water-gas shift reaction, and thus to demonstrate how sub-critical heating rate affects its generation, it is necessary to plot its yield prior to consumption at the instance when it is highest.

The results for cellulose are shown in Fig. 6a. The yield of H_2 is negligibly affected by heating rate in the 500 °C case, however, it can be seen that at 600 °C slowing the heating rate from 690 to 6.9 °C min^{-1} correlated with an increase in H_2 yield from 14.2 to 16.8 mol kg$_{dry}^{-1}$. The maximum yield of CO also increased steadily as heating rate was slowed in both temperature cases. The yields of CH_4 and CO_2 from the SCWG of cellulose are also largely unaffected by changes to the sub-critical heating rate, with the exception being a reduction in CO_2 yield from 16.7 to as the heating rate is slowed in the 500 °C case. Moreover, sub-critical heating rate was demonstrated to produce little change in the CGE, though slowing the heating rate at 600 °C did reduce the CGE from 95.5% to 93%. It can be concluded from Fig. 6a that the SCWG of cellulose is most significantly governed by reaction temperature, however, a discernible increase to H_2 yield can be achieved by slowing the sub-critical heating rate.

Fig. 6b clearly shows that a far greater correlation exists between the SCWG of hemicellulose and the sub-critical heating rate. Yields of H_2 increase drastically as the heating rate is slowed from 690 to 6.9 °C min^{-1}. Notably, in the 600 °C case the H_2 yield increased by over 42% from 33.0 to as the heating rate was slowed from 690 to 6.9 °C min^{-1}. A steady increase and decrease in the yields of CO and CH_4, respectively, was also observed for the same change to heating rate. Similarly to cellulose, slowing the heating rate in the 500 °C case appears to decrease yields of CO_2; however, the converse of this happens at 600 °C. Fig. 6b also indicates that whilst the CGE from the SCWG of hemicellulose is largely unaffected by sub-critical heating rate at 600 °C, in the 500 °C case a slower heating rate can be used to increase the CGE. In all, the results here suggest that the SCWG of high-hemicellulose, wet biomass wastes (*e.g.*, brewing wastes[25]) could be optimised by slowing the sub-critical heating rate to expedite H_2 production.

Fig. 6c indicates that lignin achieves a far lower CGE compared to cellulose and hemicellulose, and that slowing the heating rate reduces the CGE and yields of all syngas species. Protein gasifies more readily than lignin, reaching a CGE of nearly 60% at 500 °C, however, it is shown on Fig. 6d how temperature is a much more important variable and sub-heating rate has a negligible effect on the CGE and yields of all syngas species from the SCWG of protein.

3.2.2 Intermediate compounds. Fig. 7 indicates how intermediate species produced during the hydrothermal

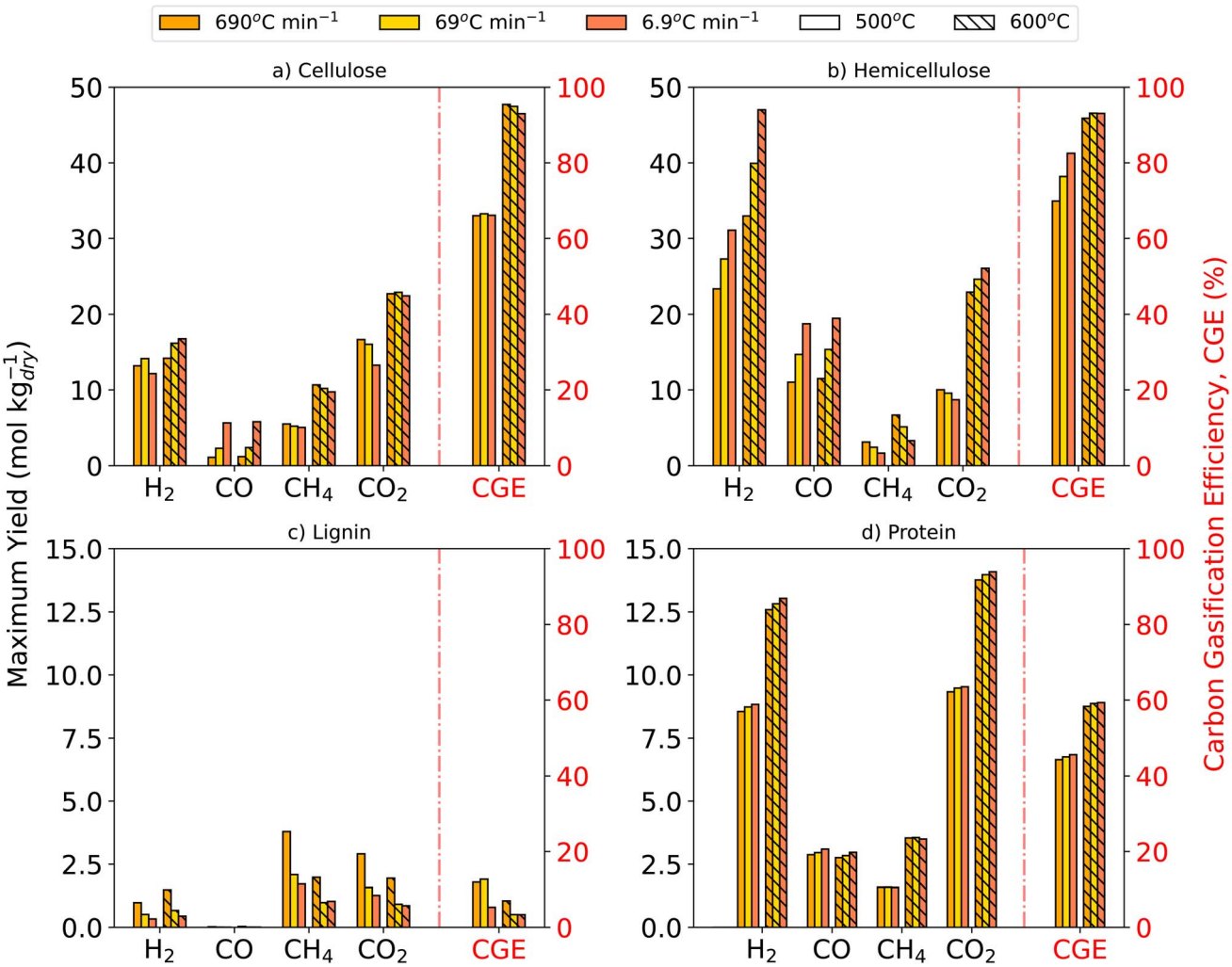

Fig. 6 Syngas yields and CGEs from the SCWG of 10 wt% (a) cellulose, (b) hemicellulose, (c) lignin, and (d) protein at 500 °C and 600 °C with linear SUB-HEX heating rates of 690, 69, and 6.9 °C min^{-1}.

decomposition of cellulose are affected by changes to sub-critical heating rate. Since the intermediate species are consumed, yields of each species presented are plotted at the instance when they are highest. Moreover, the right-hand axis shows plots the temperature at which the maximum yield occurs, to indicate how this is affected by heating rate. Not all intermediates are presented on Fig. 7, only those that occur in non-trace amounts. Fig. 7a shows that acetic, lactic, and formic acid are the most prolifically formed intermediates from the SCWG of cellulose. Both the yields of acetic and lactic acid are mainly unaffected by changes to sub-critical heating rate, whilst the yield of formic acid reduces as the heating rate is slowed. For all three species on Fig. 7a, slowing the heating rate reduces the maximum yield temperature.

Fig. 8a shows that furfural, methy formate, and glyceraldehyde all decrease in yield as the heating rate is slowed, whilst the maximum yield of WSHS increases. Additionally, slowing the sub-critical rate reduces the temperature at which the maximum yield of all species on Fig. 7a occur. Fig. 8b indicates that the formation of acetic and lactic acids is more sensitive to heating rate from a hemicellulose feedstock than what was observed for cellulose. These two species, alongside acetaldehyde, steadily decrease in yield as the heating rate is slowed. Fig. 8b also shows that the peak yield temperature of lactic acid and pyruvaldehyde are particularly affected by SUB-HEX heating rate, as it is shown that slower heating rates can be used to generate these species at lower temperatures. The peak yield temperatures of acetic and acrylic acid, and acetaldehyde are less affected by heating rate which means the production of these species is dependent on reaching higher temperatures approaching 374 °C at the end of SUB-HEX.

The intermediate compounds formed during the SCWG of lignin and protein were also studied, however, little effect was observed.

3.2.3 Char formation. Fig. 10 plots the total char formation for lignin and protein at sub-critical heating rates of 690, 69, and 6.9 °C min^{-1}, with two cases of final reaction temperature, 500 °C and 600 °C, are presented. The formation of char is plotted as a dry mass percentage *versus* total reaction time, and the reaction temperature is also plotted on the opposite *y*-axis.

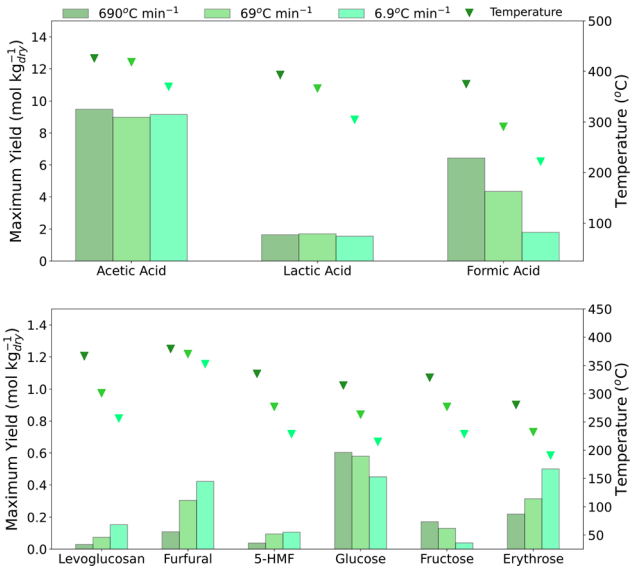

Fig. 7 Maximum yields of intermediates formed during the SCWG of cellulose with linear SUB-HEX heating rates of 690, 69, and 6.9 °C min^{-1}.

The time-scales (*x*-axis) of Fig. 10a–c is varied to ignore regions where no char formation occurs. Whilst char can be formed from cellulose and hemicellulose *via* a furfural intermediate (`fu.ch`), the generation of char from these biomass components is negligible in comparison to lignin and protein, and thus they were not discussed in this subsection.

The occurrence of char during the hydrothermal decomposition of protein is accounted for by a single reaction in the kinetic model, `as.g`, where aspartic acid is converted into glycine. Fig. 10 shows that the quantity of char produced from protein is unaffected by final reaction temperature, as the 500 °C and 600 °C plots are superimposed on top of each other. A marginal reduction to char yield can be made by slowing the heating rate, as the final dry mass fraction of char from protein decreased from 38.2% to 37.3% to 36.5% as the heating rate was slowed from 690 though to 69 and 6.9 °C min^{-1}. Fig. 10a shows that with a heating rate of 690 °C min^{-1} a maximum yield of char from protein is achieved at a temperature of around 390 °C; Fig. 10b show that this peak yield temperature reduces to around 375 °C and 320 °C as the heating rate is slowed to 69, and 6.9 °C min^{-1}, respectively.

This demonstrates that char formation from protein occurs almost exclusively in the sub-critical region and explains why no discrepancy was observed between the 500 °C and 600 °C cases. Therefore, controlling the primary decomposition of protein at cooler, sub-critical temperatures is imperative for mitigating char formation. However, since heating rates had an insignificant influence on char production from protein, varying heating rates is not effective at preferentially selecting aspartic acid decompositions reactions that do not produce char (`as.a`) over reactions that do (`as.g`).

The formation of char from lignin is far more complex in the kinetic model with contributions coming from five precursor molecules. Benzene (`b.ch`), diphenyl (`t.ch`), guaiacol (`gu.ch`), naphthalene (`na.ch`), and phenol (`p.ch`). Fig. 10a shows that with a fast sub-critical heating rate of 690 °C min^{-1}, in the 600 °C case the total formation of char increases rapidly as temperatures surpass the critical point and then steadily increase to a dry mass percentage of 33.0%. At 500 °C, the rise in char formation also commences in the supercritical region but occurs less abruptly and reaches a smaller total dry mass fraction of 22.3%. When the sub-critical heating rate is slowed to 69 °C min^{-1}, Fig. 10b again shows that char formation in notable quantities only occurs once supercritical conditions are met. At both 500 °C and 600 °C, the increase in dry mass fraction of lignin-derived char is less abrupt in comparison to the faster, 690 °C min^{-1} scenario; additionally, smaller final dry mass fractions of 15.4% and 23.4%, respectively, are achieved for the two temperature cases. Fig. 10c interestingly shows that slowing the heating rate further to 6.9 °C min^{-1} promotes the formation of char in the sub-critical region in notable quantities, with a total char dry mass fraction of over 25 % occurring after 3000 s at the end of the sub-critical zone. This slowest heating rate resulted in the greatest yield of char of all the heating rates studies, with final dry mass fractions of 39.1% and 34.2% char being reached for the 500 °C and 600 °C cases, respectively.

Sub-critical heating rate clearly has a great influence on char yields from the SCWG of lignin. However, the relationship is non-linear which is a symptom of the multiple reaction pathways for lignin char formation that exist. Given the predominance of ocresol as intermediate (see SI), its likely that the effect of heating rate on char formation is governed by the behaviour of this compound, although further investigation is required to establish the exact cause for any correlation the exists.

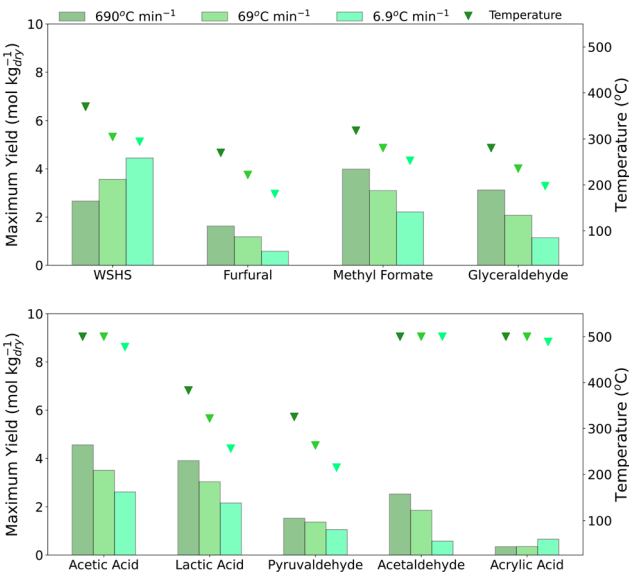

Fig. 8 Maximum yields of intermediates formed during the SCWG of hemicellulose with linear SUB-HEX heating rates of 690, 69, and 6.9 °C min^{-1}.

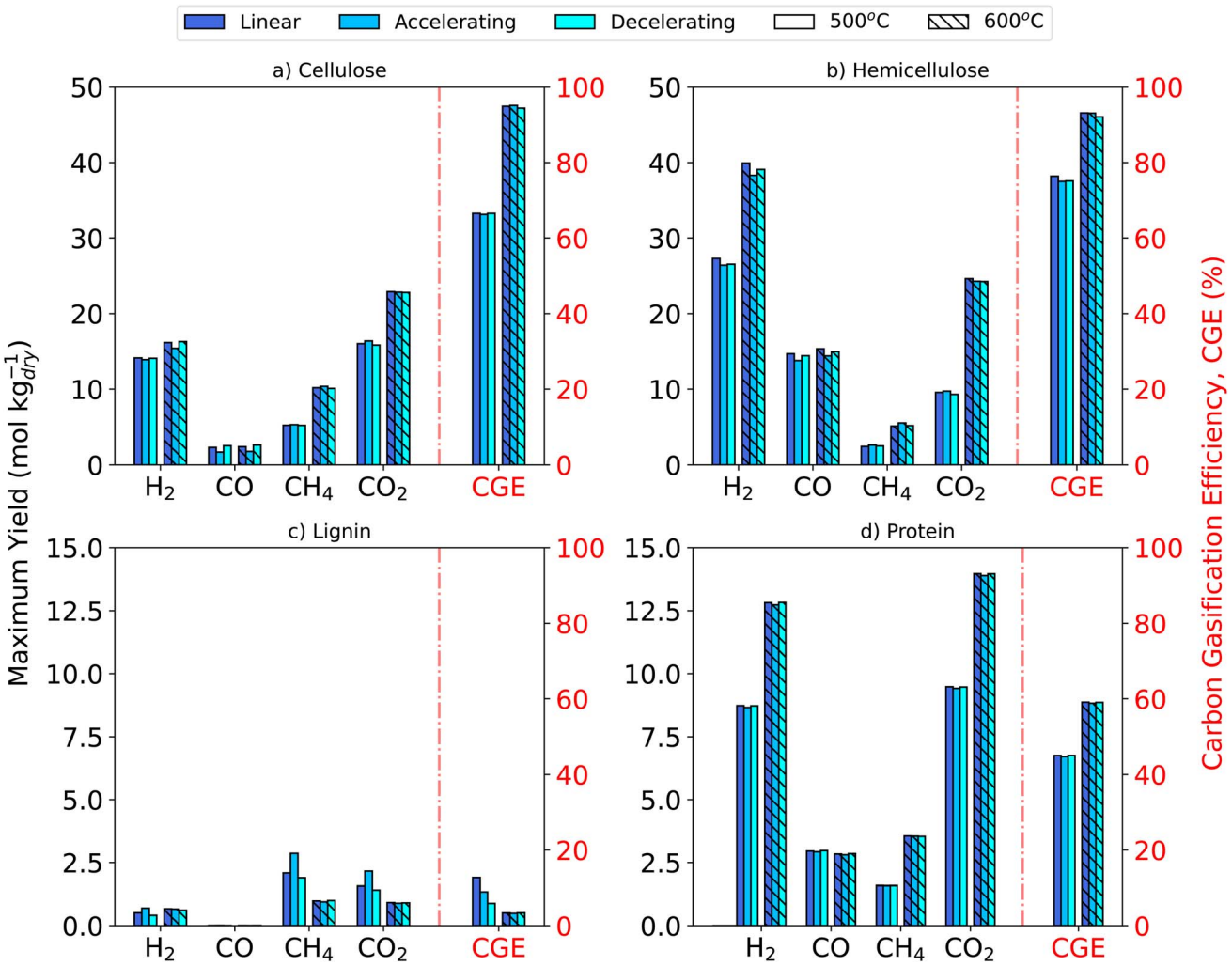

Fig. 9 Syngas yields and CGEs from the SCWG of 10 wt% (a) cellulose, (b) hemicellulose, (c) lignin, and (d) protein at 500 °C and 600 °C with linear, accelerating, and decelerating 69 °C min^{-1} SUB-HEX heating rates.

3.3 The effect of heating profile

3.3.1 Syngas yields and CGE. Fig. 9 shows how the yields of syngas species from each biomass component are affected by changes to the sub-critical heating profile at a fixed heating rate of 69 °C min^{-1}. Both Fig. 9a and b show very clearly that the CGE and yield of syngas from the SCWG of cellulose and hemicellulose, respectively, are largely unaffected by changes to heating profile at reaction temperatures of 500 °C and 600 °C. Fig. 9d similarly shows that sub-critical heating profile appears to have no influence on the SCWG of protein. Lignin was the only biomass component to demonstrate any dependence between syngas yields and heating profile. Fig. 9c suggests that at 500 °C an accelerating profile favours a greater yield of CH_4 and CO_2, whilst the CGE is highest with a linear heating at 500 °C.

3.3.2 Char formation. Fig. 11 shows that the formation of char from protein occurred exclusively in sub-critical conditions for the three heating profiles studied and a fixed heating rate of 69 °C min^{-1}, meaning no difference in result was observed between the 500 °C and 600 °C cases. There was also no significant effect of heating profile on the final yield of char from protein, with the dry mass fraction plateauing at around 37% on all three Fig. 11 plots. The maximum protein char yield was reached at a shorted residence time when using the decelerating profile as it reaches temperatures necessary for char formation sooner. The effect of heating profile on char formation was also studied at heating rates of 6.9 °C min^{-1} and 690 °C min^{-1} – see SI. Again, the only noteworthy influence was that the decelerating profile reduces the time required to reach the maximum char yield, although this effect was minimised at the faster heating rate of 690 °C min^{-1}.

Fig. 11 show that when using an accelerating profile, a greater yield of lignin-derived char is achieved at 500 °C (22.4%) case than 600 °C (22.1%). The same effect is presented on Fig. 11b for the decelerating profile with final char dry mass fractions of 33.2% and 28.8% being reached at 500 °C and 600 °C, respectively. Whilst the linear profile yields the lowest overall amount of char from lignin (15.4% and 23.4%), the results presented on Fig. 11 demonstrate that heating profile can be used to adjust the yield of char depending on the

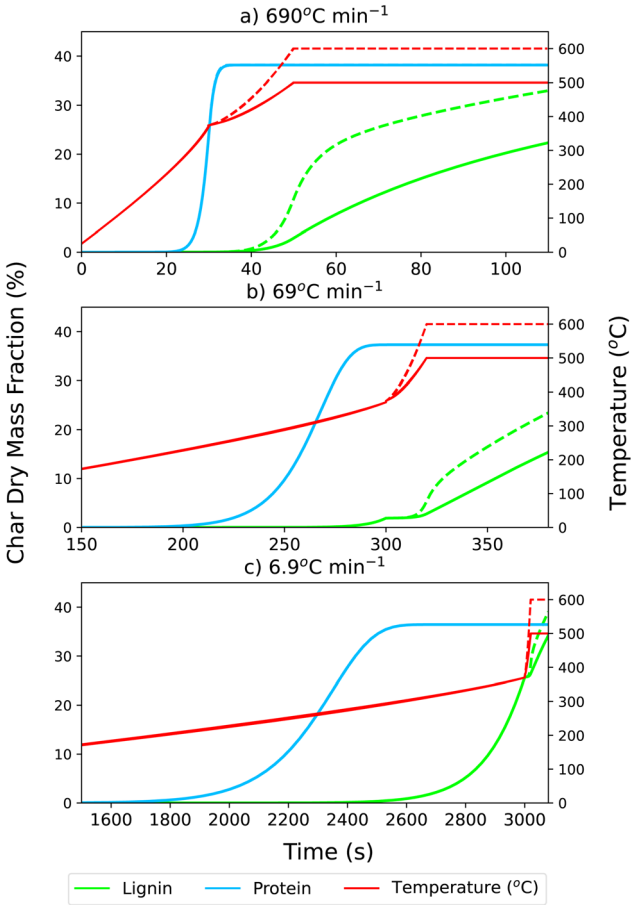

Fig. 10 Total dry mass fraction of lignin and protein derived char, and temperature, *versus* reaction time at linear sub-critical heating rates of (a) 690°C min^{-1}, (b) 69°C min^{-1}, and (c) 6.9 °C min^{-1}. Final reaction temperatures of 500 °C (solid) and 600 °C (dashed).

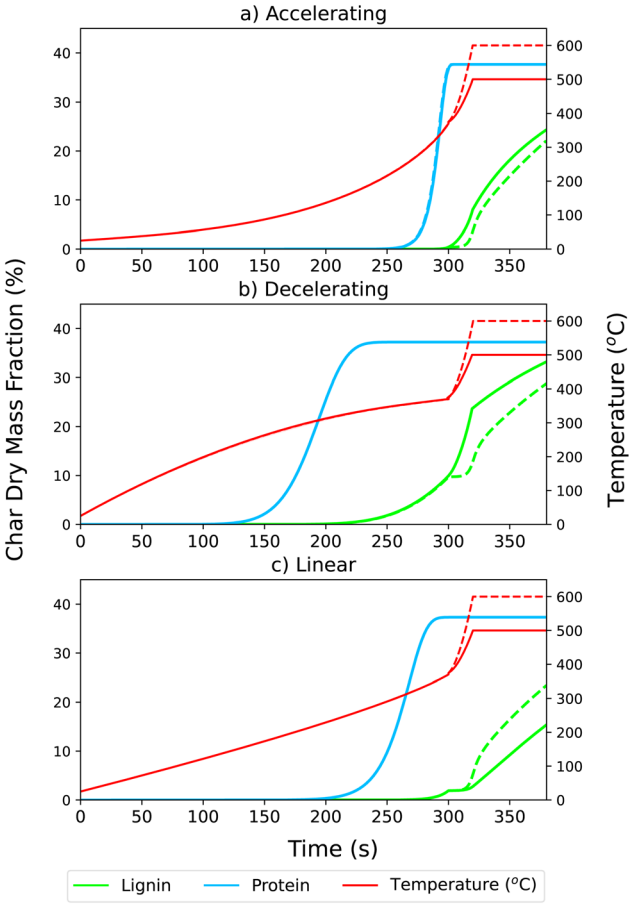

Fig. 11 Total dry mass fraction of lignin and protein derived char, and temperature, *versus* reaction time at an (a) accelerating, (b) decelerating, and (c) linear sub-critical heating rate of 69 °C min^{-1}. Final reaction temperatures of 500 °C (solid) and 600 °C (dashed).

reaction temperature. This however was not the case for heating rates of 690 and 6.9 °C min^{-1} (see SI), where neither the decelerating nor the accelerating heating profile produced greater yields of char at 500 °C.

4 Conclusions

This work has successfully advanced a detailed kinetic model and applied it to investigate how the heating rate and profile in sub-critical conditions can enhance syngas yields and suppress char formation during the SCWG of four major constituent species of real-world wet biomass: cellulose, hemicellulose, lignin, and protein.

The heating rate was found to have the most significant effect on the SCWG of hemicellulose, where slower sub-critical heating rates at both 500 °C and 600 °C led to increased H_2 yields. Longer sub-critical residence times were also found to increase the CGE in the 500 °C case. Cellulose is less sensitive to heating rate, however, slower heating rates were found to marginally increase H_2 yields at 600 °C. Faster heating rates generally increased gas yields from the SCWG of lignin. Analysing the char formation from lignin revealed that using too slow a heating rate can lead to sub-critical char formation, which results in a greater overall yield of char. However, using unnecessarily fast heating rates also lead to an increase in char yield suggesting an optimal compromise exists. Heating rate was found to have no overtly obvious effect on the final yield of syngas species or char from the SCWG of protein.

For the heating profiles studied in this work, one noteable influence was that the decelerating heating profile was found to increase the formation of char from the SCWG of lignin.

Author contributions

Robert Sait-Stewart: conceptualization, methodology, investigation, writing – original draft, visualization. Leo Lue: methodology, software, writing – review and editing, supervision. Jun Li: writing – review and editing, supervision, funding acquisition.

Conflicts of interest

The authors declare that they have no known competing financial interests or personal relationships that could have appeared to influence the work reported in this paper.

Data availability

Data is available upon request.

Supplementary information (SI) is available. See DOI: https://doi.org/10.1039/d5se00755k.

Acknowledgements

This work was supported by the Engineering and Physical Sciences Research Council (EPSRC) [grant number EP/T517938/1].

Notes and references

1 D. Meek, A. Jenevezian, R. Leishman, N. Odeh and J. Bates, *Comparing Scottish bioenergy supply and demand in the context of Net-Zero targets*, Ricardo Energy & Environment, 2022, DOI: 10.7488/era/2233.
2 C. S. Lee, A. V. Conradie and E. Lester, *Chem. Eng. J.*, 2021, **415**, 128837.
3 J. Bates, *Biomass Feedstock Availability: Final Report, Ricardo energy & environment report*, 2017.
4 J. M. Ribeiro, R. Godina, J. C. Matias and L. J. Nunes, *Sustainability*, 2018, **10**, 2323.
5 S. K. Sansaniwal, K. Pal, M. A. Rosen and S. K. Tyagi, *Renew. Sustain. Energy Rev.*, 2017, **72**, 363–384.
6 K. Alper, K. Tekin, S. Karagöz and A. J. Ragauskas, *Sustain. Energy Fuels.*, 2020, **4**, 4390–4414.
7 R. Muhlke, J.-B. Castaing, M. Morel and V. Donat, *Hydrothermal Gasification – White Paper*, 2023.
8 Y. Hu, M. Gong, X. Xing, H. Wang, Y. Zeng and C. C. Xu, *Renew. Sustain. Energy Rev.*, 2020, **118**, 109529.
9 J. A. Okolie, R. Rana, S. Nanda, A. K. Dalai and J. A. Kozinski, *Sustain. Energy Fuels.*, 2019, **3**, 578–598.
10 J. Vasco-Correa, S. Khanal, A. Manandhar and A. Shah, *Bioresour. Technol.*, 2018, **247**, 1015–1026.
11 Y. Matsumura, M. Harada, K. Nagata and Y. Kikuchi, *Chem. Eng. Commun.*, 2006, **193**, 649–659.
12 O. Farobie, P. Changkiendee, S. Inoue, T. Inoue, Y. Kawai, T. Noguchi, H. Tanigawa and Y. Matsumura, *Ind. Eng. Chem. Res.*, 2017, **56**, 6401–6407.
13 C. He, C.-L. Chen, A. Giannis, Y. Yang and J.-Y. Wang, *Renew. Sustain. Energy Rev.*, 2014, **39**, 1127–1142.
14 C. Rodriguez Correa and A. Kruse, *J. Supercrit. Fluids*, 2018, **133**, 573–590.
15 O. Yakaboylu, G. Yapar, M. Recalde, J. Harinck, K. G. Smit, E. Martelli and W. de Jong, *Ind. Eng. Chem. Res.*, 2015, **54**, 8100–8112.
16 B. M. Kabyemela, T. Adschiri, R. M. Malaluan and K. Arai, *Ind. Eng. Chem. Res.*, 1999, **38**, 2888–2895.
17 T. Flannelly, M. Lopes, L. Kupiainen, S. Dooley and J. J. Leahy, *RSC Adv.*, 2016, **6**, 5797–5804.
18 A. A. Peterson, F. Vogel, R. P. Lachance, M. Fröling, M. J. Antal Jr and J. W. Tester, *Energy Environ. Sci.*, 2008, **1**, 32–65.
19 J. Qi and L. Xiuyang, *Chin. J. Chem. Eng.*, 2007, **15**, 666–669.
20 N. Gao, K. Kamran, C. Quan and P. T. Williams, *Prog. Energy Combust. Sci.*, 2020, **79**, 100843.
21 B. Bajzelj, W. McManus and A. Parry, *Food Waste in Primary Production in the UK*, WRAP, Banbury, UK, 2019.
22 L. Tiong, M. Komiyama, Y. Uemura and T. T. Nguyen, *J. Supercrit. Fluids*, 2016, **107**, 408–413.
23 Y. Lu, L. Guo, C. Ji, X. Zhang, X. Hao and Q. Yan, *Int. J. Hydrogen Energy*, 2006, **31**, 822–831.
24 A. Nakamura, E. Kiyonaga, Y. Yamamura, Y. Shimizu, T. Minowa, Y. Noda and Y. Matsumura, *J. Chem. Eng. Jpn.*, 2008, **41**, 433–440.
25 *Phyllis2*, 2024.